Plasmonic-Tuned Flash Cu Nanowelding with Ultrafast Photochemical-Reducing and Interlocking on Flexible Plastics

Jung Hwan Park, Seungyong Han, Dongkwan Kim, Byoung Kuk You, Daniel J. Joe, Sukjoon Hong, Jeongmin Seo, Jinhyeong Kwon, Chang Kyu Jeong, Hong-Jin Park, Taek-Soo Kim, Seung Hwan Ko, and Keon Jae Lee**

Herein, a high-performance copper nanowire (Cu NW) network (sheet resistance ≈ 17 Ω sq^{-1}, transmittance 88%) fabricated by plasmonic-tuned flash welding (PFW) with ultrafast interlocking and photochemical reducing is reported, which greatly enhance the mechanical and chemical stability of Cu NWs. Xenon flash spectrum is tuned in an optimized distribution (maximized light intensity at 600 nm wavelength) through modulation of electron kinetic energy in the lamp by generating drift potential for preferential photothermal interactions. High-intensity visible light is emitted by the plasmonic-tuned flash, which strongly improves Cu nanowelding without oxidation. Near-infrared spectrum of the flash induced an interlocking structure of NW/polyethylene terephthalate interface by exciting Cu NW surface plasmon polaritons (SPPs), increasing adhesion of the Cu nanonetwork by 208%. In addition, ultrafast photochemical reduction of Cu NWs is accomplished in air by flash-induced electron excitations and relevant chemical reactions. The PFW effects of localized surface plasmons and SPPs on junction welding and adhesion strengthening of Cu network are theoretically studied as physical behaviors by finite-difference time-domain simulations. Finally, a transparent resistive memory and a touch screen panel are demonstrated by using the flash-induced Cu NWs, showing versatile and practical uses of PFW-treated Cu NW electrodes for transparent flexible electronics.

1. Introduction

Light–material interaction technologies (e.g., low-temperature polycrystalline silicon (LTPS), laser lift-off) have contributed to a tremendous breakthrough in our modern lifestyle, as they have provided powerful solutions to open a new era of electronics, such as active matrix organic light-emitting diodes (OLEDs), flexible electronics, and biomedical applications.[1–8] They provide an exceptional capability to stimulate physical/chemical reactions of nanomaterials with extremely high spatial and temporal control.[9] Successful demonstrations have been realized by using nanostructures as light-driven heat sources, enabling plasmonic welding of nanojunctions to construct high-performance optoelectronic materials and devices, including flexible touch screens, solar cells, and transparent conductors.[10–12]

A variety of light sources from lasers to lamps (continuous wave (CW) or flash) have been utilized to induce the plasmonic heating of nanomaterials.[9,12–15] However, spot-beam lasers have shown low productivity due to the time-consuming serial process.[16] The requirements of high optical energy (30 W cm^{-2} for 60 s) of CW lamps also hinder industrial application along with safety concerns.[17] From the perspective of a scalable and inexpensive light source, xenon flash lamps have attracted considerable attention because of their fast (μs to ms) and large-area processability, high output efficiency, and compatibility with roll-to-roll production.[10,14,18,19] The rapid and

J. H. Park, Dr. B. K. You, Dr. D. J. Joe, Dr. C. K. Jeong, Prof. K. J. Lee
Department of Materials Science and Engineering
Korea Advanced Institute of Science and Technology (KAIST)
291 Daehak-ro, Yuseong-gu, Daejeon 34141, Republic of Korea
E-mail: keonlee@kaist.ac.kr

Prof. S. Han
Department of Mechanical Engineering
Ajou University
San 5, Woncheon-Dong, Yeongtong-Gu, Suwon 16499, Korea

D. Kim, Dr. J. Kwon, Prof. S. H. Ko
Department of Mechanical Engineering
Seoul National University
Gwanak-gu, Seoul, Ansan, Gyeonggi-do 15588, Republic of Korea
E-mail: maxko@snu.ac.kr

Prof. S. Hong
Department of Mechanical Engineering
Hanyang University
55 Hanyangdaehak-ro, Sangnok-gu, Ansan, Gyeonggi-do
15588 Republic of Korea

J. Seo, Prof. T.-S. Kim
Department of Mechanical Engineering
Korea Advanced Institute of Science and Technology (KAIST)
291 Daehak-ro, Yuseong-gu, Daejeon 34141, Republic of Korea

Dr. H.-J. Park
BSP Co., Ltd.
126 Beolmal-ro, Dongan-gu, Anyang-si, Gyeonggi-do
14057 Republic of Korea

DOI: 10.1002/adfm.201701138

localized thermal interactions of flash light can overcome the thermal limit of flexible electronics (e.g., LTPS heat treatment on plastics above 1000 °C in a few ns). The flash light can be generated by an electrical discharge that ionizes the gas atoms with quantized energy states, causing the emission of a broad and random spectrum.[18] An unpolarized and full spectrum can simultaneously induce various photothermal properties that occur at distinct wavelength, including localized surface plasmons (LSPs) and surface plasmon polaritons (SPPs), regardless of the nanostructure arrangement.[19,20] However, flash light is difficult to tune because there are many systematic constraints (e.g., gas pressure in the flash tube, discharge capacitor, and circuit inductance of flash lamps) that correlate with the light-emitting characteristics.[18,21] This results in a fundamental limitation in controlling the ideal excitation of photothermal properties for customized plasmonic welding and adhesion strengthening.

Recently, the flash lamp techniques have achieved outstanding adaptability to metallic nanoparticles (NPs) and nanowires (NWs), facilitating simple platforms of printed electronics.[22–29] Our group also demonstrated excellent performance of an Ag nanonetwork on plastics by flash-induced interactions. Nonetheless, the high material cost and electromigration of Ag prevent the prevailing usage for widespread applications.[30–32] In this regard, considerable efforts have been devoted to replacing Ag elements with Cu for highly conductive, low electromigration, and remarkably cheap (100 times lower than Ag) electrodes, as proven by a Cu damascene process in the semiconductor industry.[33] However, Cu can be severely oxidized during photothermal interactions because of its low oxidation potential.[11] Many researchers have used various approaches, including polyol processing[34] and sonochemical reduction,[35] to repetitively reuse oxidized Cu electrodes, but none of them successfully satisfy the necessary production cost and time.

Herein, we report the plasmonic-tuned flash welding (PFW) of Cu NWs with ultrafast interlocking and photochemical reduction. The spectrum of xenon flash light was shaped in an optimized distribution through modulation of electron kinetic energy in the lamp by inducing drift potential for preferential plasmonic interactions. The high-intensity visible light from plasmonic-tuned flash enhanced self-limited nanowelding at Cu NW junctions without any oxidation, resulting in a Cu network with outstanding conductivity and transparency (sheet resistance of ≈17 Ω sq^{-1}, transmittance of 88%). The near-infrared (NIR) of flash light could thermally melt the Cu NW/PET interface and induce the interlocking structure by exciting the SPPs of Cu NWs. To investigate the adhesion enhancement of interlocked Cu NWs, we conducted a quantitative peel test to measure the NW interfacial fracture force, exhibiting 208% increased adhesion force compared to that of a pristine Cu NW electrode. Furthermore, rapid photochemical reduction of oxidation-damaged Cu NWs was demonstrated in ambient conditions for facile, repetitive, and instantaneous reuse of Cu electrodes. The PFW effect of LSPs and SPPs on junction welding and adhesion strengthening of the Cu NW network was theoretically investigated by a finite-difference time-domain (FDTD) analysis. To demonstrate the practical and versatile uses of PFW-induced Cu NW electrodes, touch screen panels (TSPs) and transparent resistive memory were fabricated by integrating the Cu NWs into functional flexible devices.

2. Results and Discussion

Figure 1a schematically illustrates the overall concept of Cu NW light interactions by PFW. Cu NWs were first synthesized by reducing copper(II) nitrate trihydrate ($Cu(NO_3)_2 \cdot 3H_2O$, Sigma Aldrich, No. 61194) through hydrothermal reactions with hydrazine solution (35 wt% in H_2O, Sigma-Aldrich, No. 309400). As shown in Figure S1 (Supporting Information), very long Cu NWs with an aspect ratio of ≈500 (a diameter of ≈100 nm, a length of ≈50 μm) were synthesized, which can provide excellent optoelectronic properties.[36] These Cu NWs were transferred by a vacuum filtration process onto either glass or PET substrates to form a Cu NW network of high sheet resistance (several MΩ sq^{-1}) caused by weak NW bonding. Upon the irradiation of a plasmonic-tuned flash, three types of light interactions (e.g., plasmonic welding, photochemical reducing, and interlocking) could occur as presented in Figure 1a-i,ii,iii. (i) The extreme fields were locally generated at the NW intersections, facilitating the junction welding for the highly conductive Cu NW network. (ii) Oxidized Cu NWs were rapidly recovered into Cu NWs by the photochemical reaction. (iii) Finally, interlocked Cu NW/PET structures could be formed through thermal melting of the interface between Cu NWs and the polymer substrate by the surface plasmon polariton (SPP) excitation, which enhances the adhesion of the Cu NW network. To provide a theoretical investigation of the PFW method, FDTD simulations were performed, as shown in Figure 1b,c. Two identical Cu NWs (with circular cross-section shape of 100 nm diameter) were piled up in perpendicular directions and illuminated by a pulse wave (wavelength from 400 to 800 nm). In order to observe the effect of photothermal local heating in the Cu NW junction, absorbed power was only integrated in the junction area (150 nm width and length and 250 nm height) with 10 nm cell size. Figure 1b shows spectral and polarization-dependent simulations of light absorption associated with heat generation of the Cu NW network from ultraviolet to visible regions. A strong peak around 600 nm was observed when the field is directed perpendicularly to the top Cu NWs, indicating that intensive heat could be produced by electromagnetic interactions. As shown in the inset of Figure 1b, this intensive field generation could be interpreted by LSP coupling at the NW junction, resulting in the welded nanojunctions. In the case of light polarized parallel to the upper Cu NWs, the plasmonic peak of Cu NWs is significantly reduced due to the light backscattering effect.[9] This welding sensitivity on the light wavelength and NW crossing angle explains the advantage of flash light over a linearly polarized laser because the former can induce intense welding regardless of randomly oriented Cu NW arrangement for further improvement of the Cu NW conductivity. The inset of Figure 1c shows that the light absorption is considerably reduced as the NWs are physically fused to each other. When the NWs are welded, the electric field in the NWs drops off and the plasmonic heat generation is decreased, showing the self-limiting nature of PFW process. These characteristics can enhance the material stability because it prevents

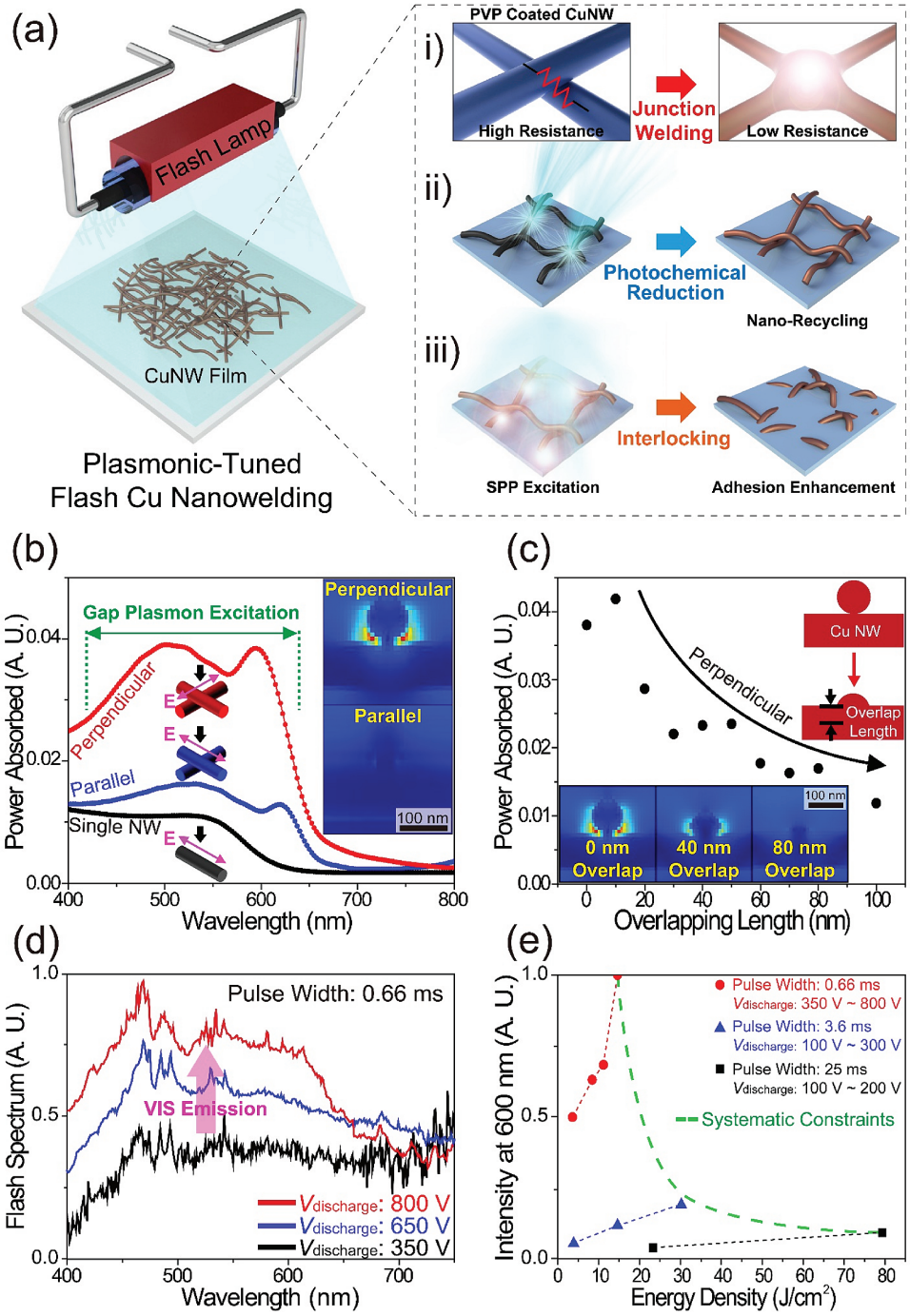

Figure 1. a) Schematic illustration of the Cu NW PFW process. b) Spectral and polarization-dependent simulations of local light absorption for the Cu NW junction from 400 to 800 nm wavelength. The inset shows the field enhancement response under the visible light (wavelength of 600 nm) for light polarized perpendicular/parallel to the first NW. c) Local heat generation as a function of Cu NW overlap length, which shows the self-limiting nature of the PFW process. The insets show field distribution simulations as a function of Cu NW overlap length. d) Normalized flash light spectrum emitted by discharging voltage of 350, 650, and 800 V at a pulse width of 0.66 ms. e) Normalized flash intensity at 600 nm wavelength emitted by various discharging voltages and pulse widths. The green dashed line indicates the systematic constraints caused by the limited power supply and capacitance of the flash lamp.

the Cu NWs from breaking up by excessive thermal shock and deterioration.[9]

Based on these Cu NW plasmonic properties, the flash spectrum tuning process was performed by modulating the discharging voltage and pulse duration of flash ignition to optimize extreme plasmonic interactions with Cu NWs. As shown in Figure 1d and Figure S2 (Supporting Information), the light spectrum at 350 V discharging voltage and 0.66 ms

pulse duration shows low-intensity visible light (wavelength from 400 to 700 nm). In contrast, the intensive visible light was emitted due to strong drift potential induced in the flash tube as the discharging voltage increases from 350 to 800 V, resulting in emission of maximized-intensity visible light at 600 nm wavelength by our flash system (detailed information regarding the flash light adjustment process can be found in the Experimental Section). It should be noted that low discharging voltages of 300 and 200 V have to be restrictedly applied for the emission of light with the pulse width of 3.6 and 25 ms, respectively, due to the limitations of the flash lamp power capacity. As a result, the long-pulsed flash irradiates visible light with much lower intensity than short-pulsed flash, and mainly emits an NIR spectrum (Figures S2 and S3, Supporting Information and Figure 1e). Through this light-tuning process, we could achieve the desirable spectrum shape corresponding to the plasmonic properties of Cu NWs in Figure 1b for efficient nanojunction welding.

The morphological evolution of PFW-welded Cu NW junctions was characterized by scanning electron microscopy (SEM) for comparison with the bulk-heated Cu NW junctions by rapid thermal annealing (RTA), as shown in **Figure 2**a,b. The plane-view SEM image of the Cu NW network heated by RTA at 300 °C in vacuum for 30 min shows the perturbed shape of Cu NWs with weak junction bonding due to the Rayleigh instability (Figure 2a).[37] As shown in Figure 2b,c, in contrast, the PFW process spontaneously induces self-limited and localized heat generation at the NW intersections within 1 ms, enabling wide and robust contact formation of the Cu network without any NW damage. The representative Cu NW network (marked by NW_1 and NW_2) in Figure 2c was further investigated by a focused ion beam (FIB) process to examine the cross section of a flash-welded intersection of Cu NWs. The NW_1 and NW_2 of 100 nm diameter were well-welded to each other without any interinsulating layer (Figure 2d). Figure 2e shows a transmission electron microscopy (TEM) image of the flash-welded Cu NWs (marked by NW_A and NW_B), revealing that the two Cu NWs are merged and firmly fused together. As shown in Figure 2f, the high-resolution TEM (HRTEM) image of the NW junction in Figure 2e (indicated as a black box) also shows that the different NW_A and NW_B are connected and coexist at the NW intersection by the PFW process. (Detailed information on the step-by-step images of the cross-sectioned NW intersection can be found in Figure S4, Supporting Information.)

Figure 2g and Figure S5 (Supporting Information) present the PFW effect on Cu NW properties of sheet resistance and transmittance after the flash exposure. The sheet resistance of the Cu NW film on glass substrates was dramatically decreased by 4–5 orders of magnitude (from 10^6 to 17 Ω sq^{-1}) after the flash irradiation with a pulse duration of 0.66 ms and energy density of 14.6 J cm^{-2} without any degradation of transparency (transmittance of 88% at 550 nm). To the best of our knowledge, this performance is the highest optoelectronic property reported for Cu-based transparent flexible conductors by light–material interactions. Interestingly, the junction nanowelding phenomena did not effectively occur when the long-pulsed light with higher energy density (28.9 J cm^{-2} at 3.6 ms, and 78.9 J cm^{-2} at 25 ms) than short-pulsed flash (14.6 J cm^{-2} at 0.66 ms) is irradiated (Figure S6, Supporting Information). It presents that PFW-induced light-focusing effect under a sub-diffraction limited scale is an essential factor for effective Cu NW welding interactions which cannot be achieved by simply raising the flash energy. Considering the synthesized NWs with different shape, diameter, length, aspect ratio, and NW gap that sensitively decrease the plasmonic reactions of Cu NWs, a greater amount of Cu NW junctions can be uniformly welded by the broadband flash light, which can induce effective plasmonic interactions regardless of NW conditions compared to laser.[9,38] The X-ray diffraction (XRD) patterns in Figure 2h reveal that the PFW-processed Cu NWs were not oxidized during high-temperature photothermal interactions due to rapid heating and cooling of Cu NWs in a millisecond.[39] In contrast, the Cu network annealed by normal thermal treatment and long-pulsed light in air was damaged by oxidation as shown in Figure 2h and Figure S7 (Supporting Information).

Figure 3a schematically illustrates the photochemical reduction process. To accelerate the oxidation of Cu NWs, we annealed the Cu NWs in ambient conditions. By irradiating the flash light in the presence of a reducing agent (i.e., ethylene glycol (EG)), the Cu_xO NWs were reduced to Cu NWs within 660 µs. This flash-induced photochemical reduction could be explained by a successive dehydration process that triggers duplicative oxidation-reduction reactions between EG and Cu_xO NWs as follows.[40,41]

$$2HO(CH_2)_2OH + Cu_xO \xrightarrow{h\nu,\ -2H_2O} 2CH_3CHO + Cu_xO \quad (1)$$
$$\xrightarrow{h\nu} CH_3COCOCH_3 + H_2O + Cu$$

Initially, EG is rapidly transformed to acetaldehyde by photonic oxidation with the first dehydration reaction through photothermal heating of Cu_xO NWs. In this regard, a xenon flash lamp is a suitable light source for efficient photothermal interactions, since most of the flash spectra have higher photonic energy than the bandgap of the Cu_xO NWs (1.2 eV). Because acetaldehyde has high reducing power, the Cu_xO NWs can be spontaneously reduced into pure Cu NWs as a chain reaction with the second dehydration, yielding the diacetyl. Furthermore, this reduction process could be significantly enhanced by electromagnetically excited electrons, which are sequentially recombined to the defect-level band states such as cationic vacancies of Cu_xO.[42]

Figure 3b shows optical photographs of Cu NWs and Cu_xO NWs in the photochemical reducing process. Color changes of Cu and Cu_xO network are conspicuously noticeable; the inherent color of Cu and Cu_xO NWs is reddish and black, respectively. EG was spin-casted on the oxidized Cu NW film, and then half of the Cu_xO NWs (remarked by black dashed lines) were covered by a shade mask to selectively reduce the Cu_xO NWs. After the flash light irradiation, the exposed part of the Cu_xO NWs was completely reduced, as shown in Figure 3b-iii. Figure 3c,d shows SEM and EDS (energy dispersive X-ray spectroscopy) mapping results of oxidized and photoreduced Cu NWs, respectively. The SEM images in Figure 3c,d show the difference in surface morphologies between oxidized and reduced Cu NWs. A rough island structure of Cu_xO NW surfaces was formed by the stress mismatch between the Cu and thermally

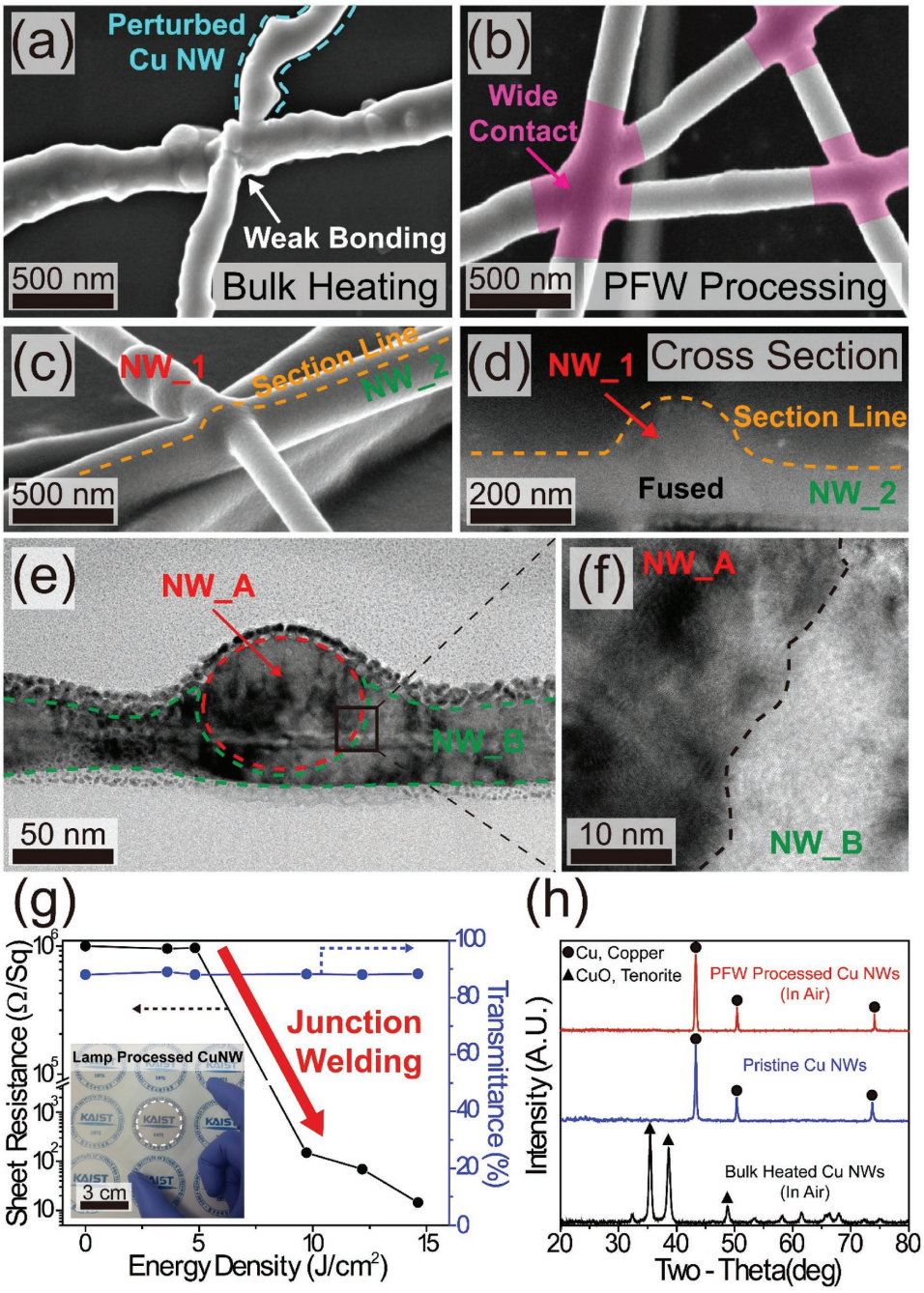

Figure 2. Morphological evolutions of bulk-heated and PFW-processed Cu NWs on a glass substrate. a) A plane-view SEM image of bulk-heated Cu NWs. b) A plane-view SEM image of PFW-treated Cu NWs. c) A tilted view SEM image of Cu NWs after PFW. d) A cross-sectional SEM image of a PFW-processed Cu NW junction enabled by the FIB-SEM procedures. e) A plane-view TEM image of fused Cu NW junction. f) HRTEM image of a welded Cu NW junction in (e). g) The sheet resistance and transmittance of Cu NW network subjected to different flash energy density. The inset shows a photoimage of the Cu NW film (on a glass substrate) after the PFW process. h) XRD patterns of the pristine, bulk-heated, and PFW-treated Cu NWs. They verify that the PFW process can fabricate high-performance and oxidation-free Cu NWs in ambient conditions, unlike the bulk heating method.

oxidized Cu_xO layer,[43] whereas the reduced Cu NWs showed a smoother surface, indicating that the oxidized Cu NWs were thoroughly reduced by photochemical interactions, as presented in the top insets of Figure 3c,d. A corresponding EDS analysis was carried out to verify the flash-induced reduction effect in terms of material composition, as shown in the bottom insets of Figure 3c,d. The EDS data show that the oxygen elements presenting throughout the entire Cu_xO NWs were successfully extracted by photochemical reduction. Figure 3e shows the XRD measurement results of Cu NWs after the photonic reducing reaction of the flash lamp processing with different energy densities of 0, 8.5, and 14.6 J cm^{-2}. As shown in

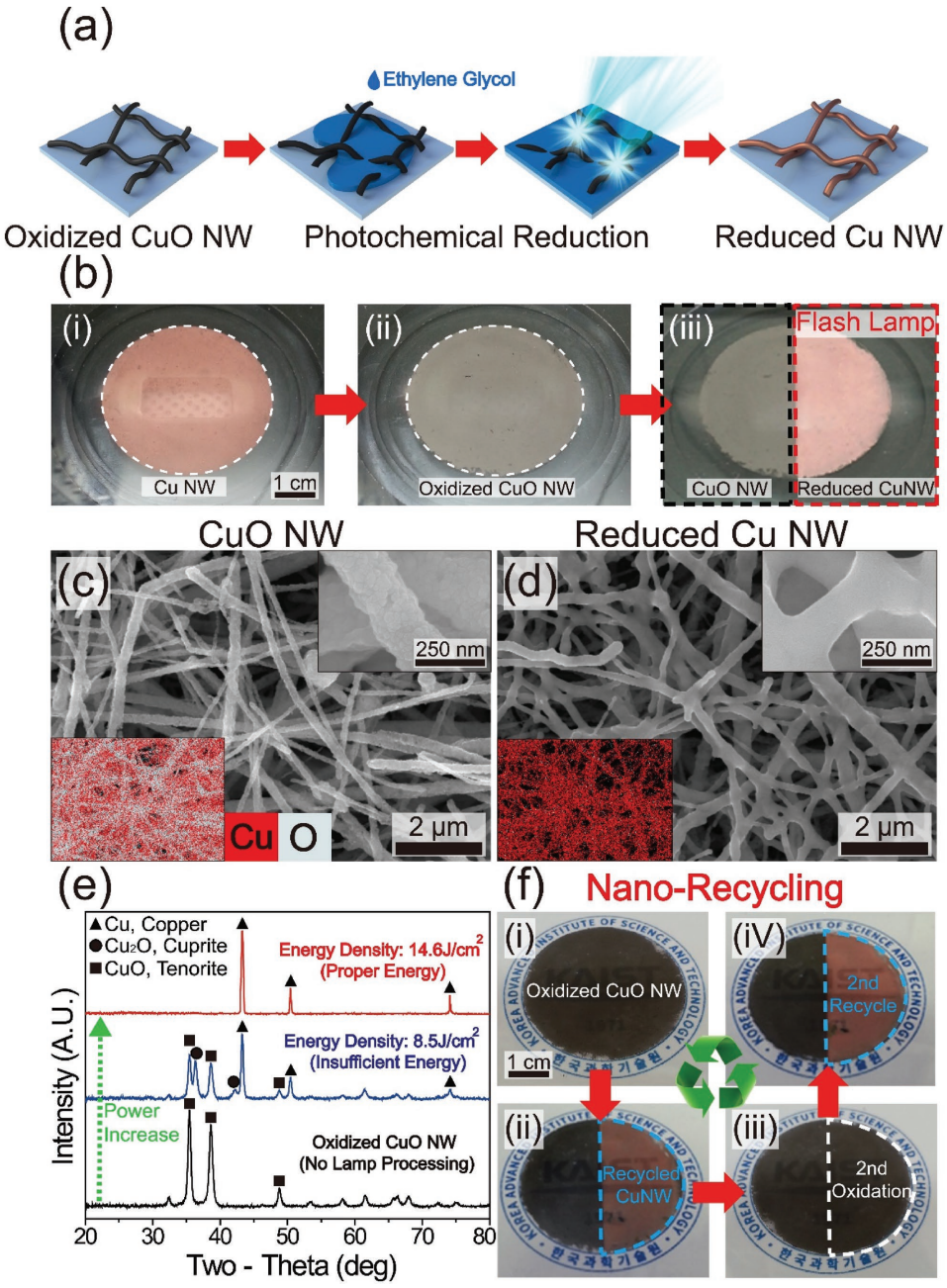

Figure 3. a) Schematic illustration of flash-induced photochemical reduction of Cu_xO NWs. b) Photographic images at each step of photochemical reducing procedures. (i) As-prepared Cu NWs, (ii) thermally induced Cu_xO NWs, and (iii) Cu_xO NWs (left-side, black) and reduced Cu NWs (right-side, reddish color) by flash lamp irradiation process. c) SEM images of pristine Cu_xO NWs. The inset (left bottom) shows EDS mapping result of Cu_xO NWs. d) SEM images of photochemically reduced Cu NWs. The inset (left bottom) shows an EDS mapping result of reduced Cu NWs by the flash lamp process. e) XRD measurements of Cu_xO NWs subjected to photochemical reduction process with different flash energy density of 0, 8.5, and 14.6 J cm^{-2}. f) Nanorecycling by reversible flash-induced photochemical reduction of Cu_xO NWs.

Figure 3e, the oxidized Cu_xO NWs were fully recovered into Cu NWs when the adequate flash light energy of 14.6 J cm^{-2} was irradiated. The large surface area could be maintained even after the reduction reactions because the agglomeration of Cu NWs only occurs at the NW junctions. Therefore, this flash-induced chemical reduction of Cu_xO NWs could be repetitively applied for a nanorecycling process (Figure 3f). Note that such repetitive photoreduction is not applicable to previous processes using NPs because the NPs are merged all together during the reduction process. The advantages of this technique are as follows: (i) the photochemical reduction can be directly employed for ultrafast repair of reoxidized Cu electrodes caused by unintentional crack of the passivation layer; (ii) Only selected parts of Cu_xO NWs can be reduced by shading the flash light with

the photomask for monolithic integration of Schottky barrier devices, including a metal–insulator–metal diode, and thin film transistors; and [44,45] (iii) This large-scale photoreduction possibly can be applied to R2R processing for cost-effective recovering processes.[10]

Figure 4a,b shows the results of FDTD simulations of SPP excitement of Cu NWs at the electromagnetic wavelength region from 800 to 1000 nm. In contrast to the gap plasmon mode in the simulation results of Figure 1b,c, the SPP could be generated at wavelength of around 900 nm for both light polarization directions, causing localized heating of NW surface. These SPP plasmonic properties could be exploited by our xenon flash lamp due to the strong NIR peak emitted by de-excitation of electrons from quantized xenon energy state, as shown in Figure S9 (Supporting Information). The thermal energy generated by the electric field at the NW surface on the plastics enables fluctuation of the PET surface (such as interlocking and embedding of Cu NWs into PET) by instantaneous melting and solidification of the polymer surface, resulting in enhanced adhesion of the Cu NW network. Consistent with the simulation results of Figure 4a,b, Figure 4c and its inset show SEM images of the Cu NW interlocking structure induced by photothermal melting of the Cu NW/PET interface through the SPP excitation.[19,20] The cross-sectional morphology of Cu NW interlocking was examined by FIB, as shown in Figure 4d. The Cu NWs locally embedded in the 100 μm thick PET surface (within the depth of 500 nm) by PFW method show fused junctions (indicated as yellow dashed line), which present the simultaneous interlocking and welding of the Cu NW network. The flash-induced interlocking of Cu NWs can enhance the interfacial fracture energy by increasing the Cu NW/PET contact area, resulting in improvement of the scratch resistance, adhesion, and lifetime of Cu NW conductors. Single-arm peel tests of Cu NW/PET specimens were conducted to verify the adhesion enhancement. 3 mm wide 3M tape was attached to the specimens and pulled by a linear actuator at a constant displacement rate of 0.5 mm s^{-1} to investigate the delamination of Cu NWs from the PET substrate. The peel strength of the flash-induced Cu NW network increases as the irradiated light energy density increases, exhibiting 208% stronger peel strength (0.5 N at 14.6 J cm^{-2}) than that of the pristine specimen (Figure 4e and Figure S11, Supporting Information). To further establish the reliability of the Cu NW electrodes, electrical resistances were also measured after quantitative peeling tests (Figure 4f). While the pristine Cu NW network was destroyed just after the first cycle of the peel test, the flash-induced Cu NW network was not disconnected after the fifth critical detaching forces, indicating that the plasmonic nanowelded Cu NWs are tough enough to endure harsh mechanical stresses. Figure 4g shows the optical transmittance of pristine and flash processed Cu NWs before and after the peel test. The original transmittance of pristine Cu NWs (41.9%–52.3% in the wavelength range from 400 to 700 nm) was increased by more than 90% after peeling, which means the adhesion of the pristine Cu NW film without flash irradiation was low enough to be detached after peeling. However, in the case of flash-processed Cu NWs, the transmittance was not increased because most of the Cu NWs firmly adhered to the polymer substrate due to flash-induced interlocking and surface embedding of Cu NWs. This effect could be clearly observed from the microscopic images of as-prepared and flash-processed Cu NWs before and after the peel test (Figure S12, Supporting Information). The mechanical stability of the flash-welded Cu NW percolations was evaluated in terms of bending deformation by monitoring the sheet resistance dependent on the radii of curvature (down to 5 mm) with repeated bending/unbending motions at 1 Hz, as shown in Figure 4h. The sheet resistance of the pristine Cu NW network increased dramatically to 1.63×10^6 Ω sq^{-1} and eventually failed at a low number of cycles (<7500). On the other hand, the sheet resistance of the flash-induced Cu NW network exhibited almost no change even after 30 000 bending cycles. This outstanding reliability and stability under the bending fatigue test was ascribed to the interlocking structure of the Cu NW/PET interface, which inhibits delamination of Cu NWs under bending.

To demonstrate the useful application of PFW-treated Cu NW electrodes for transparent and flexible electronics, we fabricated a transparent resistive memory and a TSP by employing the flash-induced Cu NW electrodes. The structure of the memory device consists of a Cu NW top electrode (TE), silicon oxide (SiO_x) solid electrolyte, and an indium tin oxide (ITO) bottom electrode (BE), as schematically illustrated in **Figure 5**a. The electrolytic insulating material (SiO_x, 100 nm) was deposited on the ITO/PET film by plasma-enhanced chemical vaporization deposition (PECVD) method at low temperature. Finally, PFW-processed Cu NWs were applied for the TE formation of a transparent and flexible resistive memory device (Figure S13, Supporting Information). As shown in Figure 5b and Figure S14 (Supporting Information), the constructed resistive memory exhibits excellent transparency (transmittance of 80% at 550 nm wavelength). Figure 5c shows the current–voltage (I–V) characteristics of the device when direct current (DC) voltage sweeping was applied to the BE (ITO) while the TE (Cu NWs) was grounded (the cell size was fixed at 100×100 μm^2). In the negative voltage sweep ranging from 0 to −2 V, the electric current increased drastically from a SET voltage of −0.5 V, exhibiting a reasonably large R_{on}/R_{off} ratio ($\approx 10^3$) by the formation of conductive filaments (CFs) from the electroforming process. The device sustained the LRS in the following sweep from −2 to 0 V but the current gradually decreased by the rupture of CFs during the positive voltage sweep from 0 to 3 V, enabling nonvolatile memory switching by controlling the growth/rupture of CFs into the insulating layer. The inset of Figure 5c,d shows the cycling endurance and bending reliability of the reset/set switching characteristics for the device at a reading voltage of −0.1 V. Despite the repeated (over 50 times) voltage sweeping and tensile bending stress (over 3000 times), the resistive memory device showed stable operation without performance degradation. Figure 5e shows a schematic illustration of the resistive TSP device, demonstrated by using PFW-processed Cu NW conductors. An ITO/PET film (Fine Chem, 15 Ω sq^{-1}) and the PFW-induced Cu NWs on PET were used as a counter electrode for the TSP. Spacers were located between the conductors to prevent an electrical short. The total active area is a circle with a diameter of 4 cm formed by the Cu NW percolation network. When the surface of the ITO/PET film was pressed by a pen, the deformed top conducting layer was connected to the bottom Cu NW network on PET, which provides information

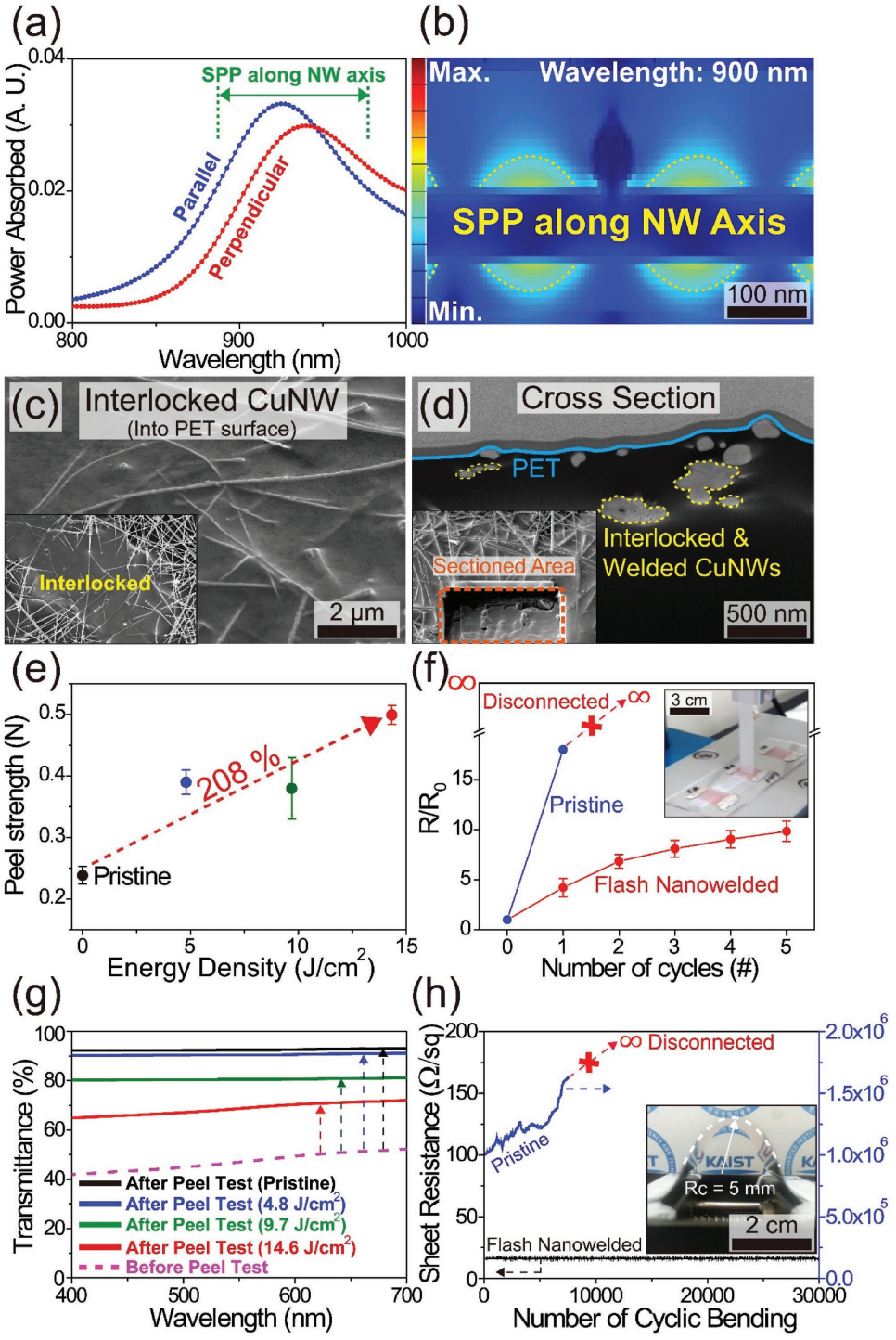

Figure 4. a) Spectral and polarization-dependent simulations of light absorption for the Cu NWs from 800 to 1000 nm wavelength. b) Field distribution response under the NIR light (wavelength of 900 nm), which shows SPP excitation mode. c) Top-view SEM image of the interlocked Cu NWs on a PET substrate by SPP-induced processing. The inset shows the plane-view SEM image of Cu NW/PET interlocking structure with low magnification. d) A cross-section SEM image of PFW-processed Cu NWs on PET substrate. The inset shows the cross-section SEM image of PFW-treated Cu NW network. e) The peel strength measurement of as-prepared (0.24 N) and PFW-treated Cu NW films (0.5 N) evaluated by the quantitative peel test. f) The normalized resistance results after peel test (from first cycle to fifth cycle) for pristine and flash-nanowelded Cu NWs. The inset shows a photographic image of the peeling test system. g) The transmittance of as-prepared and flash light processed Cu NW (at the energy density of 4.8, 9.7, and 14.6 J cm^{-2}) networks before and after peel test. h) The sheet resistance of pristine and PFW-processed Cu NW network under a cyclic bending test (bending radius: 5 mm, bending frequency: 1 Hz). The inset shows a photographic image of the Cu NW film in the bending state.

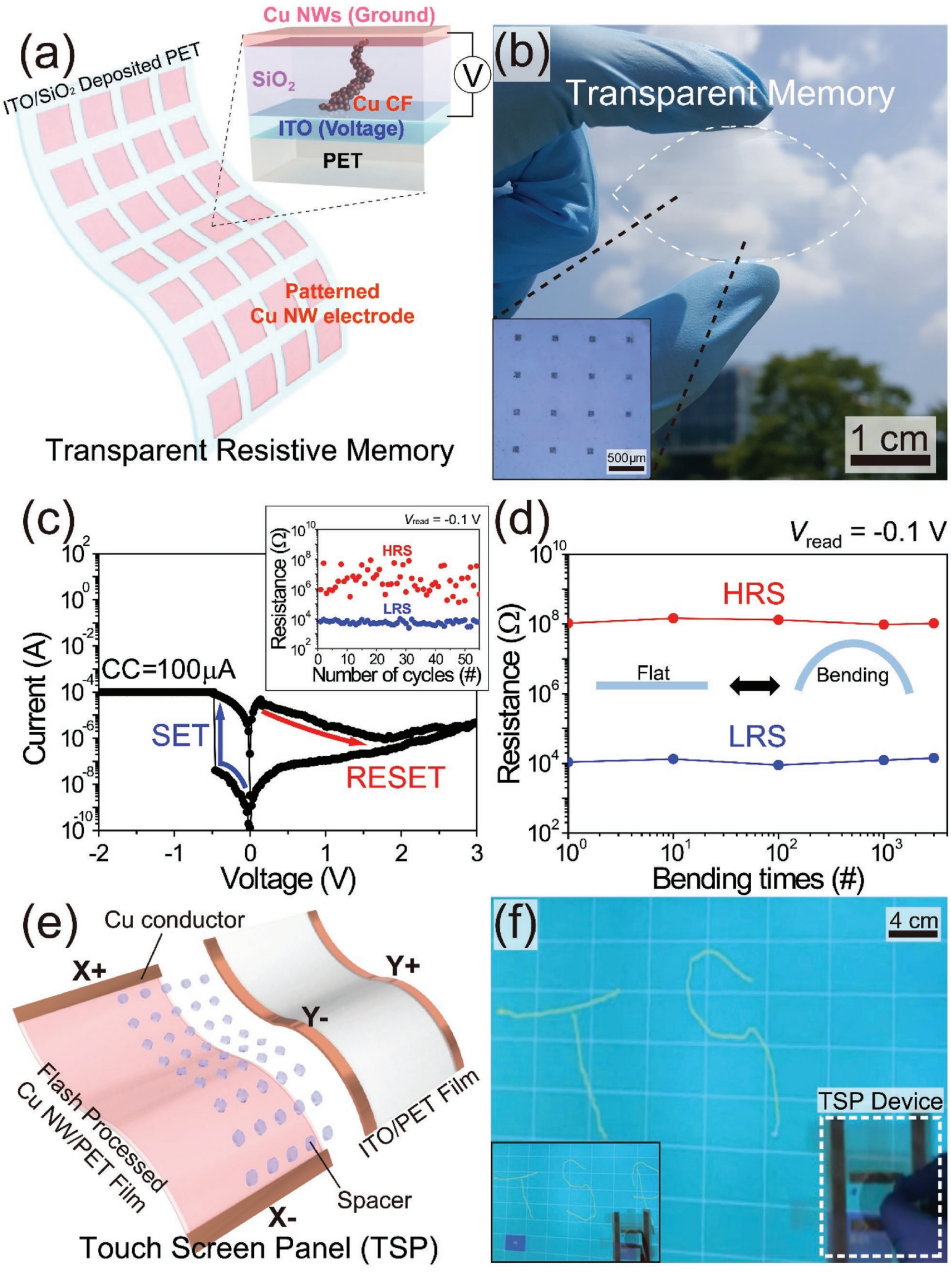

Figure 5. a) Schematic illustration of the transparent resistive memory demonstrated by using flash-induced plasmonic-welded Cu NW conductors. b) Optical image of the transparent and flexible resistive memory device. The inset shows the patterned Cu NW electrodes on the SiO_2 deposited ITO/PET substrate. c) *I–V* characteristics of the transparent memory device. The inset shows the endurance cycles of the resistive memory under –0.1 reading voltage. d) The ON/OFF current characteristics of the transparent and flexible device under bending stresses. e) Schematic illustration of resistive TSP device. f) Demonstration of the TSP fabricated by using a PFW-processed Cu NW conductor.

of the pressured position on the device. As shown in Figure 5f, the TSP operated well according to the pen writing motion, showing the letters "TSP" on the screen. Movie S1 (Supporting Information) shows the highly sensitive TSP, which is ascribed to the excellent conductivity of the PFW-processed Cu NW conductors. These successful demonstrations of resistive memory and a TSP verify that the PFW-induced Cu NWs can be practically integrated in not only transparent materials but also flexible sensor devices.

3. Conclusions

In summary, we have presented PFW-induced Cu NWs with excellent optoelectronic properties for ultrafast interlocking and photochemical reduction. The xenon flash light was tuned to the desired distribution by controlling the drift kinetic energy of the electrons to maximize the preferential plasmonic interactions. A high discharging voltage of 800 V at a short pulse duration of 0.66 ms was applied to strongly accelerate the

electrons for intense collisions and ionization reactions between the electrons and xenon gas, resulting in high-intensity visible light (from 400 to 650 nm wavelength). The intensive visible light by plasmonic-tuned flash (power density of 14.6 J cm^{-2}) enhances self-limited local junction welding of Cu NWs without any oxidation, decreasing the sheet resistance of the Cu network (17 Ω sq^{-1} at transmittance of 88%) by 4–5 orders of magnitude. Simultaneously, the SPP excited by NIR could thermally melt the Cu NW/PET interface and improve the adhesion force between the Cu NWs and plastic substrates, exhibiting 208% higher adhesion of Cu NW conductors than the adhesion of as-prepared Cu NWs. This strong adhesion of Cu NWs provided considerable bending stability over 30 000 cycles. The FDTD simulations theoretically confirmed that junction nanowelding and adhesion strengthening of Cu NWs could occur by visible (wavelength from 600 to 650 nm) and NIR (wavelength from 900 to 975 nm) light, respectively. Furthermore, ultrafast (≈660 µs) photochemical reduction of Cu_xO NWs was demonstrated in air by irradiating the flash light with a reducing agent, causing the recovery of electrode conductivity. Using the high-performance PFW-processed Cu NWs, we demonstrated a transparent resistive memory and a TSP. The resistive memory device exhibited excellent transparency (transmittance of 80% at 550 nm wavelength) and a reasonably large R_{on}/R_{off} ratio (≈10^3) with highly reliable bending stability. Our TSP device with PFW-treated Cu NWs also showed highly sensitive operation according to the external mechanical pressure. Through the demonstration of transparent resistive memory and TSP, we show that the PFW-processed Cu NW network can be universally implemented for fully integrated flexible and transparent electronics.

4. Experimental Section

Flash Light Tuning Process: To evaluate the light-emitting characteristics, the spectrum was divided for a normalizing process by the highest intensity value of light discharged from the xenon flash lamp (from wavelength of 400 to 1000 nm). At low discharging voltage of 350 V, insufficient drift potential induced in the flash tube causes low acceleration of electrons, resulting in weak excitation of xenon gas atoms, and emission of low-intensity visible light. When high discharging voltage (800 V) is applied, the highly accelerated electrons in the flash lamp effectively ionize xenon atoms to upper energy states[18] by strong collisions between the electrons and gas atoms. This mechanism leads to high energy photon irradiation (visible light at 600 nm wavelength) with maximized intensity.

Cu NW Synthesis: In a typical synthesis, Cu NWs were synthesized by reducing copper(II) nitrate ($((CuNO_3)_2)$, Sigma Aldrich, No. 61194) with hydrazine solution (35 wt% in H_2O, Sigma-Aldrich, No. 309400). First, two deionized (DI) water based solutions were prepared: a Cu precursor and an alkaline solution. In the Cu precursor solution, 0.75 g of copper(II) nitrate was dissolved in 4 g of water. For the alkaline solution, 45 g of sodium hydroxide (NaOH, Sigma Aldrich, No. 306576) and 80 g of DI water were mixed in a flask with a magnetic stirring bar. During the stirring process, the temperature of the solution was automatically increased due to its exothermic reaction. After the reaction, the temperature was decreased to 60 °C when at rest. The Cu precursor solution, 650 µL of ethylenediamine (EDA, Sigma Aldrich, No. 391085), and 100 µL of hydrazine solution were then added into the flask sequentially while it was being mixed. The color of the solution, which originally was royal blue, became transparent. At the moment of color change, the flask was heated in an oil bath at 60 °C for 1 h without any stirring. After this hydrothermal synthesis, reddish copper nanowires could be synthesized on the surface. The floating copper nanowires were centrifuged at 2000 rpm for 5 min, and this process was repeated five times using a DI water dispersion. Finally, the resultant Cu NWs were dissolved in isopropanol (99.5% Sigma Aldrich, No. 278475).

Vacuum Filtration and Transfer Process: Before filtering Cu NWs, a NW solution was prepared by dispersing required amount of nanowires into 20 mL of IPA. After setting up a Teflon filter (SterliTech, 47 mm in diameter with 0.2 µm pore size) on a suction base, the vacuum pump was turned on. Then, 30 mL of IPA and the prepared Cu NW solution were poured sequentially. After the filtration, the wet Teflon filter with Cu NW percolation was dried at room temperature. When the filter was completely dried, a substrate was put on the filter for 30 min with a vacuum suction. After tearing off the filter, the Cu NW film was obtained on the given substrate.

Resistive Memory Device Fabrication: ITO/PET sheets (Sigma Aldrich, No. MKBK 1894V) were prepared as substrates for the transparent resistive memory. SiO_2 (thickness of 100 nm) was deposited on the substrate by a PECVD method. The synthesized Cu NWs were vacuum transferred onto the film and patterned by a photolithography process using AZ 5214 photoresist (Figure S13, Supporting Information). Finally, the PFW process was employed to fabricate highly conductive and adhesive Cu NW electrodes to demonstrate a transparent and flexible memory device.

Materials Characterizations: The morphologies of Cu NWs were observed by using SEM (Magellan 400, FEI company), FIB-SEM (Helios Nanolab 450 F1, FEI Company, Kaist Analysis Center for Research Advancement (KARA)), and TEM (Tecnai TF 30 ST, FEI Company, Kaist Analysis Center for Research Advancement (KARA)). The chemical and elemental composition of Cu and Cu_xO NWs were monitored by using XRD (K-Alpha, Thermo Fisher Scientific) and EDS (Magellan 400, FEI company). The transmittance of the Cu NW film and transparent resistive memory were characterized by a UV–vis spectrometer (Evolution 220, Thermo Fisher Scientific). Electrical characterizations were performed by using a Keithley 4200-SCS (DC voltage/current sweep).

Supporting Information

Supporting Information is available from the Wiley Online Library or from the author.

Acknowledgements

J.H.P. and S.H. contributed equally to this work. This research was supported by the Creative Materials Discovery Program through the National Research Foundation of Korea (NRF) funded by the Ministry of Science, ICT and Future Planning (Grant No. NRF-2016M3D1A1900035), and a grant from the National Research Foundation of Korea (NRF) funded by the Korean Government (MSIP) (Grant No. NRF-2016R1A5A1009926) as well as the Nano Material Technology Development Program through the NRF funded by the Ministry of Science, ICT and Future Planning (Grant No. NRF-2016M3A7B4905609) and by National Research Foundation of Korea (2017R1A2B3005706). Figure 1, 2, 3 and the Acknowledgements were updated on August 4, 2017 following initial online publication.

Conflict of Interest

The authors declare no conflict of interest.

Keywords

interlocking, photoreducing, plasmonic-tuned flash copper nanowelding, resistive memory, touch screen panels

Received: March 1, 2017
Revised: April 6, 2017
Published online: May 29, 2017

[1] M. F. El-Kady, V. Strong, S. Dubin, R. B. Kaner, *Science* **2012**, *335*, 1326.
[2] W.-H. Chung, H.-J. Hwang, S.-H. Lee, H.-S. Kim, *Nanotechnology* **2013**, *24*, 35202.
[3] M. F. EL-Kady, R. B. Kaner, *Nat. Commun.* **2013**, *4*, 1475.
[4] S. Hong, H. Lee, J. Lee, J. Kwon, S. Han, Y. D. Suh, H. Cho, J. Shin, J. Yeo, S. H. Ko, *Adv. Mater.* **2015**, *27*, 4744.
[5] H. E. Lee, S. Kim, J. Ko, H.-I. Yeom, C.-W. Byun, S. H. Lee, D. J. Joe, T.-H. Im, S.-H. K. Park, K. J. Lee, *Adv. Funct. Mater.* **2016**, *26*, 6170.
[6] K. L. Lin, K. Jain, *IEEE Electron Device Lett.* **2009**, *30*, 14.
[7] D. V. Palanker, M. S. Blumenkranz, D. Andersen, M. Wiltberger, G. Marcellino, P. Gooding, D. Angeley, G. Schuele, B. Woodley, M. Simoneau, N. J. Friedman, B. Seibel, J. Batlle, R. Feliz, J. Talamo, W. Culbertson, *Sci. Transl. Med.* **2010**, *2*, 1.
[8] T. Shimoda, Y. Matsuki, M. Furusawa, T. Aoki, I. Yudasaka, H. Tanaka, H. Iwasawa, D. Wang, M. Miyasaka, Y. Takeuchi, *Nature* **2006**, *440*, 783.
[9] E. C. Garnett, W. Cai, J. J. Cha, F. Mahmood, S. T. Connor, M. G. Christoforo, Y. Cui, M. D. McGehee, M. L. Brongersma, *Nat. Mater.* **2012**, *11*, 241.
[10] D. Angmo, T. T. Larsen-Olsen, M. Jørgensen, R. R. Søndergaard, F. C. Krebs, *Adv. Energy Mater.* **2013**, *3*, 172.
[11] J. H. Park, S. Jeong, E. J. Lee, S. S. Lee, J. Y. Seok, M. Yang, Y. Choi, B. Kang, *Chem. Mater.* **2016**, *28*, 4151.
[12] J. A. Spechler, C. B. Arnold, *Appl. Phys. A* **2012**, *108*, 25.
[13] S. Hong, J. Yeo, G. Kim, D. Kim, H. Lee, J. Kwon, H. Lee, P. Lee, S. H. Ko, *ACS Nano* **2013**, *7*, 5024.
[14] J. Perelaer, R. Abbel, S. Wünscher, R. Jani, T. Van Lammeren, U. S. Schubert, *Adv. Mater.* **2012**, *24*, 2620.
[15] J. Yeo, S. Hong, D. Lee, N. Hotz, M.-T. Lee, C. P. Grigoropoulos, S. H. Ko, *PLoS One* **2012**, *7*, 1.
[16] M. Takai, D. Bollmann, K. Haberger, *Appl. Phys. Lett.* **1994**, *64*, 2560.
[17] H. Lu, D. Zhang, X. Ren, J. Liu, W. C. H. Choy, *ACS Nano* **2014**, *8*, 10980.
[18] a) M. Csele, *Fundamentals of Light Sources and Lasers*, Wiley, Hoboken, NJ **2004**, *1*, pp. 1–344; b) http://optdesign.narod.ru/book/Fundamental_light_source_and_lasers.pdf (accessed: July 2004).
[19] J. H. Park, G.-T. Hwang, S. Kim, J. Seo, H.-J. Park, K. Yu, T.-S. Kim, K. J. Lee, *Adv. Mater.*, **2017**, *29*, 1603473
[20] V. D. G. Jorik, S. Pierpaolo, P. Albert, *Nano Lett.* **2012**, *12*, 3138.
[21] *High Performance Flash and Arc Lamps*, Perkin Elmer Optoelectronics, Wiesbaden, Hessen **2013**, Vol. 44, p. 1.
[22] J. S. Kang, J. Ryu, H. S. Kim, H. T. Hahn, *J. Electron. Mater.* **2011**, *40*, 2268.
[23] D. J. Lee, S. H. Park, S. Jang, H. S. Kim, J. H. Oh, Y. W. Song, *J. Micromech. Microeng.* **2011**, *21*, 125023.
[24] J. Jiu, M. Nogi, T. Sugahara, T. Tokuno, T. Araki, N. Komoda, K. Suganuma, H. Uchida, K. Shinozaki, *J. Mater. Chem.* **2012**, *22*, 23561.
[25] M. Hösel, F. C. Krebs, *J. Mater. Chem.* **2012**, *22*, 15683.
[26] H.-J. Hwang, W.-H. Chung, H.-S. Kim, *Nanotechnology* **2012**, *23*, 485205.
[27] K. Mallikarjuna, H.-J. Hwang, W.-H. Chung, H.-S. Kim, *RSC Adv.* **2016**, *6*, 4770.
[28] J. Xu, Y. Wang, X. Qi, C. Liu, J. He, H. Zhang, H. Chen, *Angew. Chem., Int. Ed.* **2013**, *52*, 6019.
[29] R. Wang, H. Zhai, T. Wang, X. Wang, Y. Cheng, L. Shi, J. Sun, *Nano Res.* **2016**, *9*, 2138.
[30] H. M. Naguib, B. K. Laurin, *IEEE* **1979**, *2*, 196.
[31] A. R. Rathmell, S. M. Bergin, Y.-L. Hua, Z.-Y. Li, B. J. Wiley, *Adv. Mater.* **2010**, *22*, 3558.
[32] G. K. Dalapati, S. Masudy-Panah, S. T. Chua, M. Sharma, T. I. Wong, H. R. Tan, D. Chi, *Sci. Rep.* **2016**, *6*, 20182.
[33] P. C. Andricacos, C. Uzoh, J. O. Dukovic, J. Horkans, H. Deligianni, *IBM J. Res. Dev.* **1998**, *42*, 567.
[34] K. J. Carroll, J. U. Reveles, M. D. Shultz, S. N. Khanna, E. E. Carpenter, *J. Phys. Chem. C* **2011**, *115*, 2656.
[35] N. A. Dhas, C. P. Raj, A. Gedanken, *Chem. Mater.* **1998**, *10*, 1446.
[36] R. M. Mutiso, M. C. Sherrott, A. R. Rathmell, B. J. Wiley, K. I. Winey, *ACS Nano* **2013**, *7*, 7654.
[37] M. E. Toimil-Molares, A. G. Balogh, T. W. Cornelius, R. Neumann, C. Trautmann, *Appl. Phys. Lett.* **2004**, *85*, 5337.
[38] T. Gao, P. W. Leu, *J. Appl. Phys.* **2013**, *114*, 063107.
[39] S. Han, S. Hong, J. Ham, J. Yeo, J. Lee, B. Kang, P. Lee, J. Kwon, S. S. Lee, M.-Y. Yang, S. H. Ko, *Adv. Mater.* **2014**, *26*, 5808.
[40] F. Fievet, J. P. Lagier, B. Blin, *Solid State Ionics* **1989**, *32*, 198.
[41] S. Han, S. Hong, J. Yeo, D. Kim, B. Kang, M.-Y. Yang, S. H. Ko, *Adv. Mater.* **2015**, *27*, 6397.
[42] T. H. Fleisch, G. W. Zajac, J. O. Schreiner, *Appl. Surf. Sci.* **1986**, *26*, 488.
[43] C. Gattinoni, A. Michaelides, *Surf. Sci. Rep.* **2015**, *70*, 424.
[44] S. Jeong, H. C. Song, W. W. Lee, H. J. Suk, S. S. Lee, T. Ahn, J.-W. Ka, Y. Choi, M. H. Yi, B.-H. Ryu, *J. Mater. Chem.* **2011**, *21*, 10619.
[45] M. Abdel-Rahman, M. Syaryadhi, N. Debbar, *Electron. Lett.* **2013**, *49*, 4.

